Influence of leakage current density on the stability of Sb_2O_3 doped ZnO-V_2O_5-Bi_2O_3-MnO_2 based varistor ceramics during the DC and thermal stress

Dahiru Umaru and Miftahu Gambo Idris

Department of Physics, Faculty of Science, Yobe state university, Damaturu

**Corresponding author E-mail*: dahiruumaru8@gmail.com
(Received 15 June 2023, Accepted 22 July 2023, Published 27 July 2023)

Abstract

This study investigated the influence of DC-thermal stress on the stability of Sb_2O_3 doped ZnO–V_2O_5–Bi2O3–MnO_2 based varistor ceramics from 0 to 1 mol%. The materials were processed using a conventional solid-state technique. The samples were characterized using XRD, SEM, and EDX techniques. The use of XRD and EDX analyses related to those cited in the literature confirmed the presence of $Zn_7Sb_2O_{12}$, $MnVO_4$, $BiVO_4$, and $Zn_3(VO_4)_2$ polymorphs as the secondary phase including ZnO hexagonal wurtzite structure and MnO_2 as a primary phase. The EDX analyses reveal the presence of the $Zn_7Sb_2O_{12}$ spinel phase located at the triple point junctions, nodal point, and embedded in ZnO bulk grains. Henceforth, the results showed that Sb_2O_3 doping can improve the stability of the varistor ceramics, particularly in the phase formation of $Zn_7Sb_2O_{12}$. This contributed to good stability of Sb_2O_3 doped ZVBM varistor ceramics in terms of degradation rate coefficient of $2.02x10^{-7}$ mA $h^{1/2}$ which was accompanied by low leakage current density around -67%, largest barrier height of 1.54%, breakdown field of 69.83% and α around 72.94%.

Keywords: Varistor, Sb_2O_3, ZVBM, ceramics, Leakage current density

1. INTRODUCTION

ZnO-based varistors ceramics are well described as those electronic ceramic devices that are typically functioning to protect electronic circuits against unwanted voltage surges [1]. The varistor current-voltage (I-V) characteristics before the breakdown field displayed high resistance and low resistance after the breakdown field at which it becomes highly conductive. Besides this, the fabrication of ZnO varistor ceramic alone is associated with many difficulties which the addition of small quantities of metal oxides with heavy ionic radius. Their segregation to the grain boundary resulted in the formation of the Schottky barrier, such heavy oxides include; Sb_2O_3, Co_3O_4, Bi_2O_3, Cr_2O_3, V_2O_5, etc., are required. Generally, ZnO grain growth is well controlled by the addition of Sb_2O_3 additive it is considered that the additive affects the formation of $Zn_7Sb_2O_{12}$ spinel phase

which is responsible for reducing the grain boundaries mobility and obstructing the grain growth and also improves stability [2]. Microstructurally, ZnO varistors are composed of many grains and grain boundaries, which are uniformly distributed throughout the ceramics depending on the type of sintered ceramic and the additive used.

Another feature of ZnO varistor ceramics that are not thoroughly investigated is their multi-additive degradation phenomena. In practical application, when a ZnO varistor is exposed to a constant electrical or thermal stress the varistor degraded due to the constant leakage current and resultant watt loss [3].

The degradation of ZnO varistor electrical properties is associated with the applied stress. Many reports have shown that the grain boundary barriers decreased when there is a change in the valance band of additive atoms and the distribution of electrons and holes close to the grain boundaries. This is ascribed to the voltage and thermal energy used as responsible for the movement of defective ions within the grain or on grain boundaries. Consequently, the varistor electrical stability together with nonlinear characteristics is the major importance of ZnO varistor ceramics [4][5][6]. However, some reports reveal that such electrical properties can be enhanced when SiO_2 and Sb_2O_3 are added to ZnO varistors [7], and $Zn_{2.23}Sb_{0.67}O_4$ spinel particles are well contributed to the varistor electrical degradation reduction [8]. Other than the impurities, thermal treatment can also enhance the varistor electrical degradation [9][10]. Yet, the effect of heat treatment is not clear with regard to the enhancement of electrical degradation due to the impurities. Generally, the Sb_2O_3 additive has an influence on ZnO varistor ceramics positively. Hence, in ZnO varistor ceramics' electrical degradation, critical clarification on the effect of the Sb_2O_3 additive is highly significant.

Numerous research works have been carried out on the effect of Sb_2O_3 doping on varistor stability in different systems, but the influence of leakage current density on the stability of Sb_2O_3 doped ZVBM-based varistor ceramics during DC and thermal stress have not been reported yet. In this work, our primary hypothesis is how the amount of Sb_2O_3 additive would influence the leakage current for the best stability of ZVBM-based varistor ceramics. To get optimum stability, various sintering temperatures on a sample without Sb_2O_3 were performed. Further investigation on the effect of Sb_2O_3 doped ZVBM based varistor ceramics on the degradation of electrical properties as associated to ZnO grain size using scanning electron microscope (SEM), type of elemental composition (EDX), phase identification (XRD).

2. EXPERIMENTAL PROCEDURE

A high-quality purity of metal oxide powders was carefully selected for the varistor fabrication. The powders were obtained from Sigma-Aldrich and (99.9%) ZnO, (99.6%) V_2O_5, (99.98%) -Bi_2O_3, (99.6%) Sb_2O_3, and (86.93%) MnO_2. The percentage composition is (0.2 mol. %) V_2O_5, (0.7 mol. %) Bi_2O_3, (0.7 mol. %) MnO_2, and (0 – 1 mol. %) Sb_2O_3. The raw materials were mixed by ball-milling with zirconia balls in a polypropylene bottle for 24 h in acetone and a small addition of

deionized water to avoid the sedimentation of heavy particles like Sb_2O_3. 0.75wt% polyvinyl alcohol binder that was 88% hydrolyzed and an average MW of 88000 was added. The mixture was dried at 110 °C for 19 h in an oven and crushed by means of agate mortar/pestle. The powder was sieved using 75 micro mesh screens to produce the starting powder. The powder was pressed into discs (pellets) of a 10 mm diameter and 1 mm thickness at a pressure of 50 MPa. The pellets were sintered at 1250 °C in air and 4 h holding time, with constant heating rates of 5 °C/min, and finally, furnace-cooled to room temperature. The sintered samples were polished to 0.89 mm thickness using SiC paper, P1200. Finally, the silver paste was coated on both faces and then they were heated at 550 °C for 12 min with electrode areas of approximately 0.238 cm^2 to form ohmic contacts.

3. CHARACTERIZATION METHOD

The electrical characterization J-E of the samples was recorded at room temperature by using a source measure unit (Keithley 2400) to determine the nonlinear coefficient (α). The varistor electric field (E_{1mA}) was evaluated at 1-10 mA/cm2 current density, and the leakage current density (J_L) was evaluated at $0.85V_{1mA}$. The α was obtained using the expression below: [11]

$$J = KE^{\alpha} \tag{1}$$

where J is the current density, E is the applied electric field, and a is the constant

$$\alpha = \frac{(\text{Log } J^2 - \log J^1)}{(\text{Log } E2 - \log E1)} \tag{2}$$

with, $J_1 = 10$ mA/cm^2 and $J_2 = 1$ mA/cm^2

The DC degradation tests were done for a continuous tress of 0.85E1mA/120 °C/18h. The leakage current was recorded after each 5 min concurrently using measurement unit meter Keithley 2400 during the stress time. Furthermore, the degradation rate coefficient K_T was calculated using the expression $I_L = I_{L0} + K_T t^{1/2}$, where I_L is leakage current at stress time (t) and I_{L0} is I_L at t = 0. The J-E characteristics were measured at room temperature after the stress.

Scanning electron microscope (SEM, JEOL JSM-6400) together with energy dispersive X-ray (EDX) were used to determine the ceramic microstructure structure and elements within the composition. The XRD patterns of the prepared samples were recorded by using (PANalytical X'Pert Pro PW3040/60, Philips). The samples were radiated with Ni-filtered CuKα radiation (λ = 1.5428) within a 2θ scan range of 20-80 °C to identify the crystalline phases; the data were analyzed using X'Pert High Score software. The density of the sintered pellets was measured with a digital electronic densitometer, and the average grain size was calculated by using the linear intercept method [12],[13].

$$D = 1.56L/(MN) \tag{3}$$

where L is the random line length on the micrograph, M is the micrograph magnification and N is the number of grain boundaries intercepted by lines.

4. RESULTS AND DISCUSSION

4.1 Effect of thermal treatment on the phase identification

Figure 1 (a) shows the XRD patterns of the undoped sample sintered at (1200–1300 °C) for the reference sintering temperature and (b) represents the Sb_2O_3 doping level on ZVBM samples. The patterns indicate the presence of two main phases such as ZnO hexagonal structure and MnO_2 (ICSD code: 00-011-0055). However, $MnVO_3$ (ICSD code: 00-024-1246), $BiVO_4$ (ICSD code: 00-012-0293) and $Zn_3(VO_4)_2$ (ICSD code: 00-034-0378) are the secondary phases identified. The intensity peaks related to V-species decreased with the increase in sintering temperature [14], illustrated in Figure 1 (a, b), this is probably due to the volatility of V-species at high sintering temperature and high doping level of Sb_2O_3 content. The presence of $Zn_7Sb_2O_{12}$ secondary spinel phase was observed with the doping level up to 1 mol% (figure 1b) thus, the intensity peaks are very weak maybe this is due to the small concentration of the metal oxides [15].

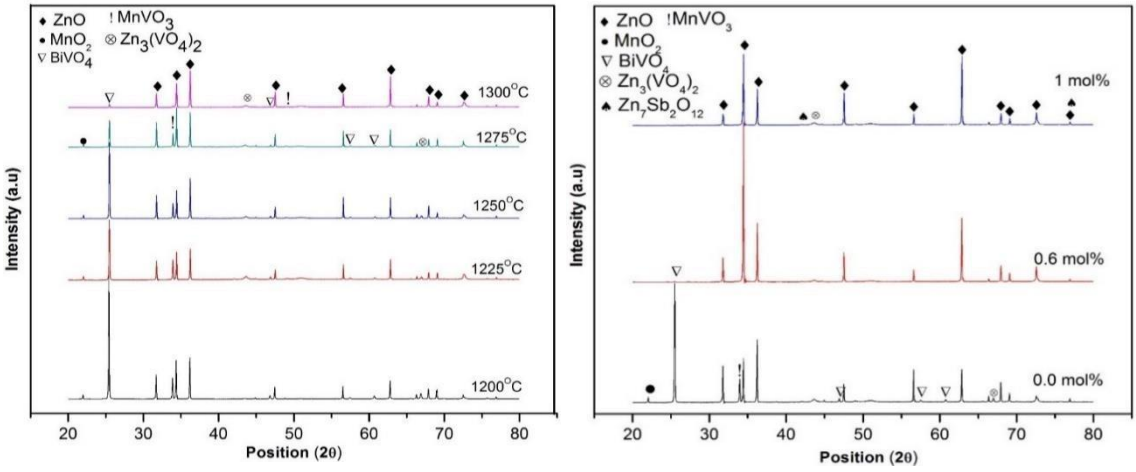

Figure 1 (a): XRD pattern of sample sintered at various temperatures; (b) Sb_2O_3 doped ZVBM varistor ceramics sintered at 1250 °C

5. MICROSTRUCTURE CHARACTERIZATIONS

Figure 2 (a, b, and c) shows the overall SEM microstructure of the undoped and x mol% Sb_2O_3 content sintered at 1250 °C. It can be observed that the microstructure of the ceramic demonstrates the presence of small grains exists at the grain boundaries and triple point junctions of ZnO bulk grains. The average grain size increase gradually and the relative density decrease with the incorporation of 0.6 and 1 mol% Sb_2O_3 (Figure 3), the reduction of relative density is attributed to the presence of pores [16].

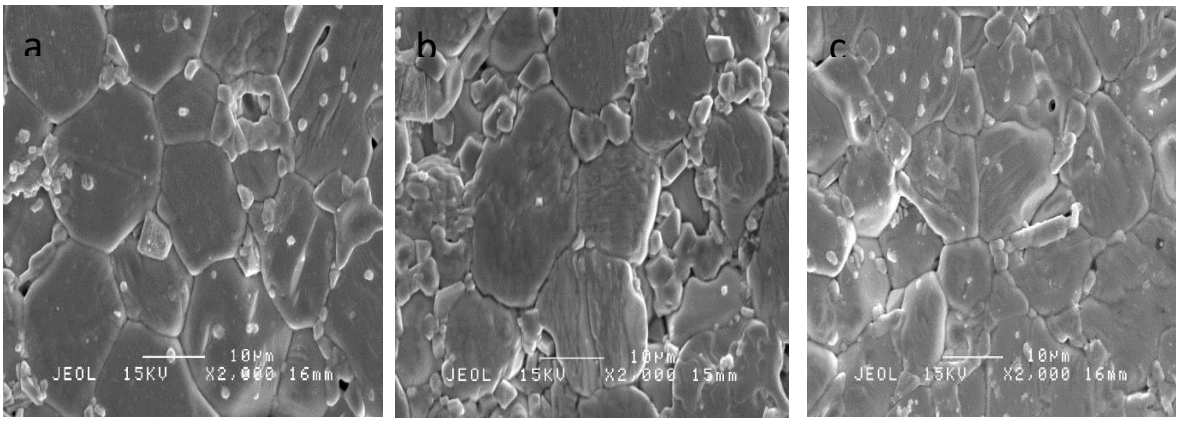

Figure 2: SEM micrograph of Sb_2O_3 doped ZVBM varistor ceramics sintered at 1250 °C (a) 0 mol% (b) 0.6 mol% and (c) 1 mol%.

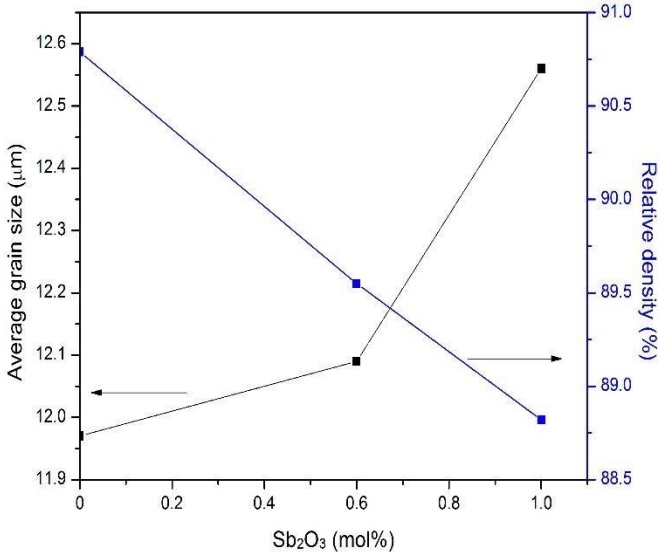

Figure 3: Average grain size, percentage density against molSb_2O_3 doped ZVBM varistor ceramics sintered at 1250 °C

Figure 4, shows the EDX spectra of ceramic with 1 mol% Sb_2O_3 doped ZVBM varistor ceramics.
It was reported that Sb exists only on grain boundary [7] which is opposed to the present finding.
In this work Sb-species was located at the nodal point, grain boundary, and ZnO grain interior (spectrum 1, 2, and 3). No peak related to Mn-species diffuses in ZnO grain interiors maybe this is due to the differences between ionic radii of Mn^{2+} (0.80 Å) and Zn^{+} (0.74 Å) [17]. Although, the presence of Mn at the grain boundary and the nodal point is a clear indication that the Mn species diffuses in the ZnO grain interior [18]. However, the presence of Sb, V, and Bi species are observed to exist at the grain boundary and nodal point of the ZnO grain (spectrum 2 and 3) [18], [19]. The existence of Sb-species at the grain boundary and nodal point substantially contributes to the inhibition of grain growth by forming the $Zn_7Sb_2O_{12}$ spinel phase [19].

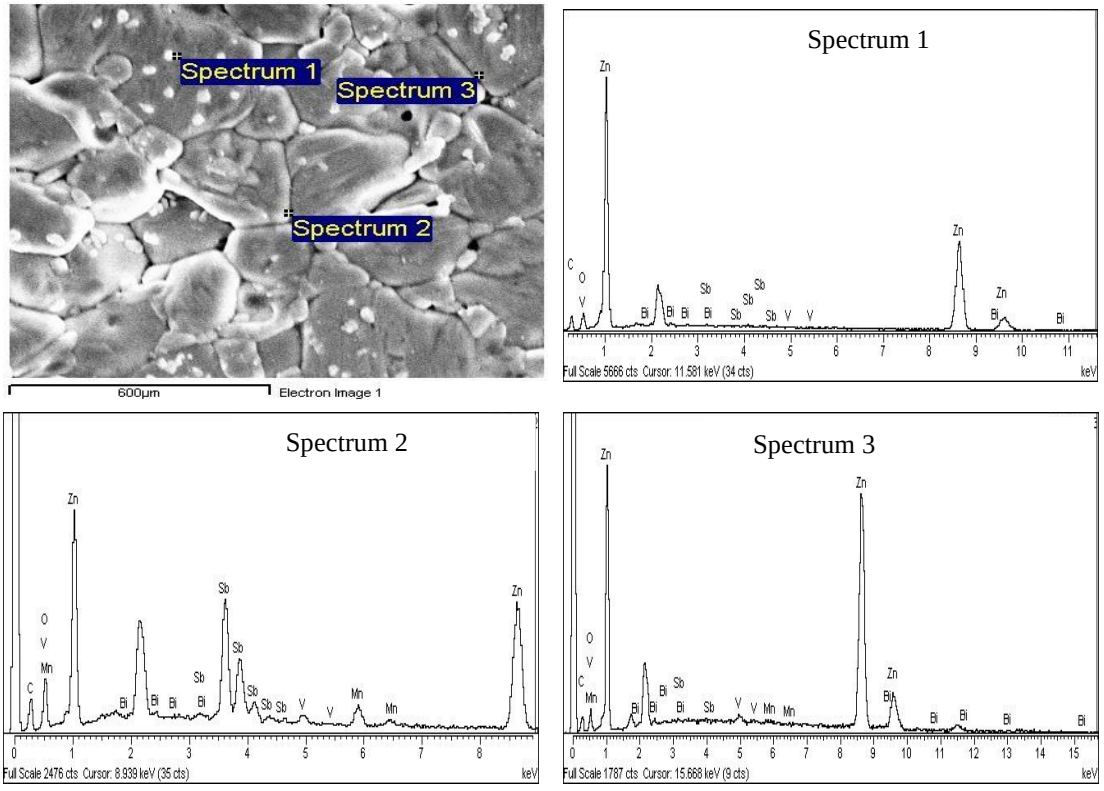

Figure 4: EDX analysis for 1mol% Sb_2O_3 doped ZVBM varistor ceramics sintered at 1250 °C.

6. ELECTRICAL CHARACTERIZATION

6.1 J-E CHARACTERISTIC CURVES OF THE VARISTOR

Figure 5(a) shows the J-E characteristic of the undoped sample with sharp switching curves and the doped sample with broader sharps. The α values decrease suddenly from 15.09 to 7.97 with the addition of Sb_2O_3 up to1 mol% through the application of 1250 °C of sintering temperature this is attributed to the increase of J_L from $1x10^{-3}$ to $3x10^{-3}$ mA/cm^2, may be due to the high thermionic emission of current during the heating process as shown in Table 1. As a result, the breakdown field decreased from 67.75 to 42.95 V/mm, similar behavior was reported by Jiang et al., 2013 [20]. Although, Sb_2O_3 doping in ZVBM varistor ceramics is mainly for two reasons; to control the grain growth by forming a secondary spinel phase of $Zn_7Sb_2O_{12}$, and enhance the solubility of ions such as Zn in Bi_2O_3-rich liquid phase. This is essential for defect distribution form at the grain boundaries during cooling reported by [21]. on the other hand, the decrease in α values implies that the solubility of Zn in the V-rich liquid phase is not enhanced by the Sb_2O_3 doping in ZVBM varistor ceramics also reported by [22]. It can be realized that the low barrier height is due to the substitution reaction which produces electrons and enhances the donor concentration. As a result, the barrier

height decreased and the varistor nonlinearity reduced as shown in Figure (5b). The lower the barrier height is the smaller the α value [20].

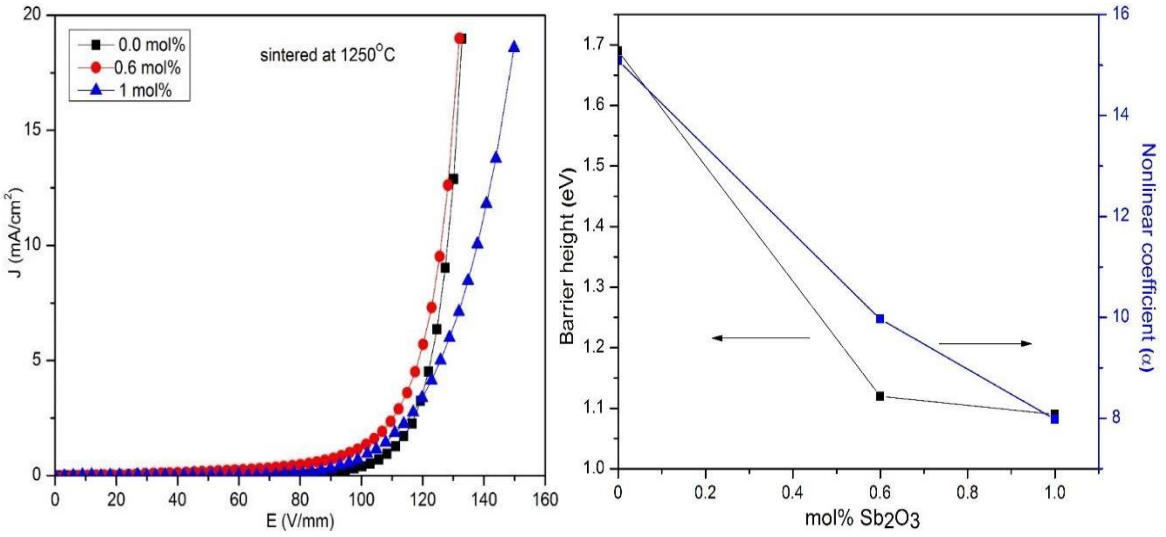

Figure 5 (a): J-E characteristic curves of Sb_2O_3 doped ZVBM varistor ceramics and (b) nonlinear coefficient, barrier height against mol% sintered at 1250 °C.

Table 1: Average grain size, percentage density, and nonlinear electrical properties of ZVBM varistor ceramics sintered at 1250 °C

Composition (mol%)	D (μm)	ρ (%)	ϕ_b (eV)	E_b (V/mm)	J_L (mA/cm^2)	α
0.0	11.97	90.79	1.69	67.75	$1x10^{-4}$	15.09
0.6	12.09	89.55	1.12	50.26	$2x10^{-4}$	9.97
1.0	12.52	88.82	1.09	42.95	$3x10^{-4}$	7.97

Figure 6 shows J_L the results of Sb_2O_3 doped ZVBM-based varistor ceramics sintered at 1250 °C and exhibited different stability during the stress of $0.85E_{1mA}$/120 °C/18 hrs. Although, the stability of the undoped sample is largely affected by high J_L after subjecting the ceramic against DC and thermal stress with a degradation rate coefficient (K_T) of $8.62x10^{-6}$ $mAh^{1/2}$ (Figure 2), low stability is related to the high J_L per grain boundary [23] and too much distribution of secondary phases [24] as shown in XRD analysis Figure 1a. It can be observed that with small doping of 0.6 mol%, the K_T gradually improves which is relatively stable with a K_T value of 5.8 $x10^{-7}$ $mAh^{1/2}$. It is evidently revealed that the varistor ceramics doped with 1 mol% Sb_2O_3 have shown the best stability having a K_T value of $2.02x10^{-7}$ $mAh^{1/2}$ after the application of DC and thermal stress, illustrated in Table 2, no thermal runway was recorded. From the macroscopic point of view, low leakage current, even

grain size, and good barrier height significantly contribute to ZnO varistor ceramics' stability with the incorporation of rare earth oxides [25]. However, high leakage current density rises the carrier generation caused by joule heat and results in a repetition cycle between joule heating and leakage current [26]. The number of conduction paths reduces due to sintered density and eventual concentration of current.

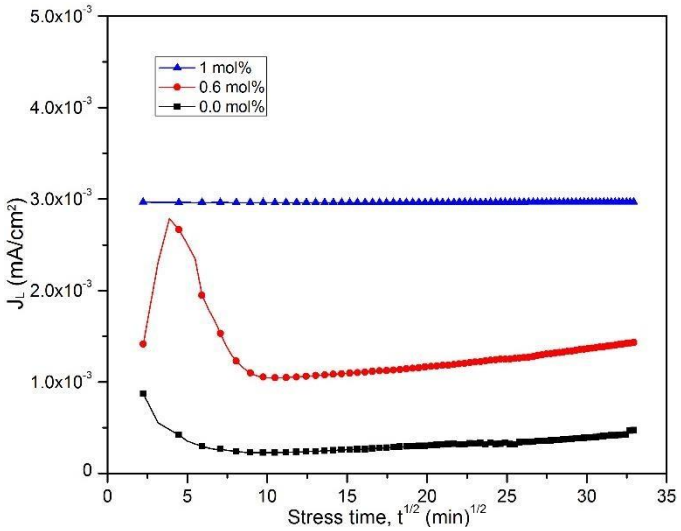

Figure 6: Leakage current against stress time during DC accelerated aging stress of sample sintered at various temperatures; (b) x mol% Sb_2O_3 sintered 1250 °C.

Figure 7 (a, b, and c) shows the relation between J-E characteristic curves' behavior before and after the stress of three different mixes. It can be seen that the curves have shown a significant variation at the pre-breakdown region with the doping level of Sb_2O_3 from 0-1 mol%. The variation changes in nonlinearity (%$\Delta\alpha$), barrier height (%$\Delta\phi$), breakdown voltage (%ΔE_{1mA}), and leakage current density (%ΔJ_L) of the samples sintered at 1250 °C are shown in Table 2. The undoped sample shows a little variation shift in J-E curves this is probably due to the high leakage current and the presence of many secondary phases [27]. The sample doped with 0.6 mol% Sb_2O_3 displays a low variation rate in terms of %ΔE_b around -11.78%, %$\Delta\phi_b$ -9.82, and %$\Delta\alpha$ -16.45 after the DC and thermal stress. It is adequate to state that the varistor ceramic prepared with 0.6 mol% Sb_2O_3 shows good stability, although there is no significant change in the electrical properties. The stability of the ZnO varistor is estimated from the K_T value from a degradation point of view [28]. In this work, the best stability is observed from the sample containing 1 mol% Sb_2O_3 doping which suppressed the J_L by -67%, possessing K_T value of 2.02×10^{-7} $mAh^{1/2}$, α improved by 78.97%, ϕ_b increase by 41.28% and the E_b increased to 69.83%. As was hypothesized best stability was obtained from the sample containing 1 mol% doping level which is in contrast to the undoped sample and 0.6 mol%. Thus, J-E characteristic curves of the varistor ceramic lose their non-opacity slowly with the applied field leading to the varistor electrical degradation [29]. Among the possible reasons for varistor electrical properties to degrade is associated with the interstitial Zn^{2+} ions or drift motion of O^{2-} ions when voltage is applied. As a result, they migrate inside the grains near the grain boundaries leading

to the distribution of holes and electrons near the grain boundaries, hence deforming the symmetric double Schottky barriers [30], [31] [32].

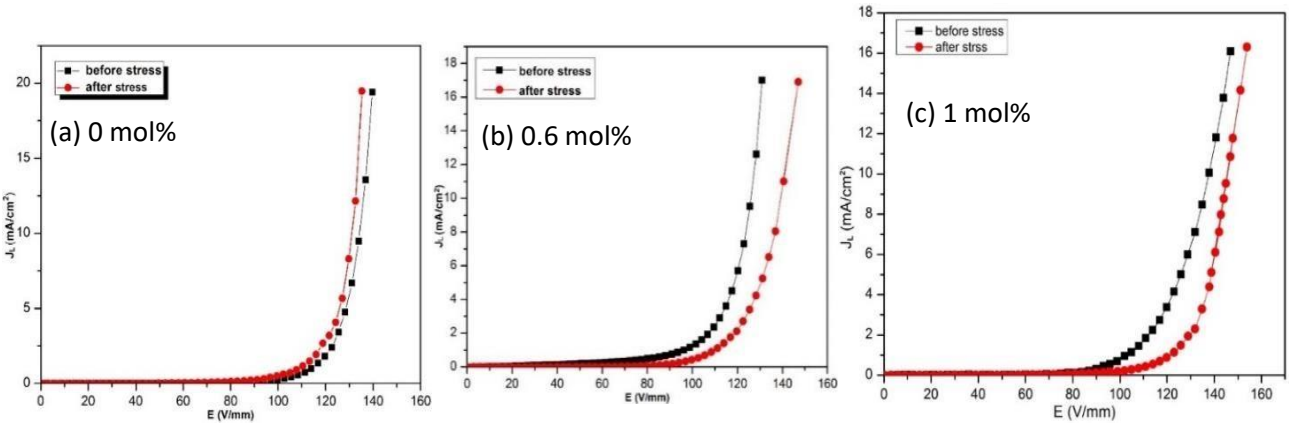

Figure 7: J-E characteristic curves before and after DC accelerated aging stress of x mol% Sb_2O_3 sintered at 1250 °C.

Table 2: Variation change in nonlinear electrical properties, before and after stress and K_T values of $Sb_2O_{3(0-1)}$ doped ZVBM varistor ceramics sintered at 1250 °C

composition (mol%)	Stress stage	K_T (mA $h^{1/2}$)	(α)	%Δα	ϕ_b (eV)	%Δϕ_b	E_b (V/mm)	%ΔE_b	J_L (mA/cm^2)	%ΔJ_L
0	Initial		15.09		1.69		67.75		$1.0x10^{-4}$	
	stressed	$8.62x10^{-6}$	6.47	-57.12	0.81	-52.07	21.23	-68.66	$3.0x10^{-3}$	200
0.6	Initial		9.97		1.12		50.26		$2.0x10^{-4}$	
	stressed	$5.8x10^{-7}$	8.33	- 16.45	1.01	-9.82	44.34	-11.78	$3.0x10^{-3}$	50
1.0	Initial		7.37		1.09		42.95		$3.0x10^{-4}$	
	stressed	$2.02x10^{-7}$	13.19	78.97	1.54	41.28	72.94	69.83	$1.0x10^{-3}$	-67

7. CONCLUSION

The influence of DC-thermal stress on the stability of Sb_2O_3-doped ZVBM-based varistor ceramics was successfully investigated. Five different sintering temperatures were initially selected, and 1250 ^oC was the optimum before doping Sb_2O_3. Then at this temperature through varying Sb_2O_3 1 mol% was observed to give the best stability possessing K_T value around $2.02x10^{-7}$ $mAh^{1/2}$ accompanied by low J_L of -67%, largest ϕ_b of 1.54%, E_b of 69.83% and α around 72.94%.

Acknowledgment

The authors are grateful to Yobe State University for supporting this work.

References

[1] S. Anas, R. V. Mangalaraja, M. Poothayal, S. K. Shukla, and S. Ananthakumar, "Direct synthesis of varistor-grade doped nanocrystalline ZnO and its densification through a step sintering technique," *Acta Mater.*, vol. 55, no. 17, pp. 5792–5801, Oct. 2007.

[2] S. Bernik, S. Maček, and A. Bui, "The characteristics of ZnO-Bi_2O_3-based varistor ceramics doped with Y_2O_3 and varying amounts of Sb_2O_3," *J. Eur. Ceram. Soc.*, vol. 24, no. 6, pp. 1195–1198, 2004.

[3] S. So and C. Park, "Improvement in the Electrical Stability of Semiconducting ZnO Ceramic Varistors with SiO_2 Additive," *J. Korean Phys. Soc.*, vol. 40, no. 5, pp. 925–929, 2002.

[4] A. Vojta and D. R. Clarke, "Microstructural origin of current localization and "puncture'' failure in varistor ceramics," *J. Appl. Phys.*, vol. 81, no. 2, p. 985, 1997.

[5] C.-S. Chen, C.-T. Kuo, and I.-N. Lin, "Improvement on the degradation of microwave sintered ZnO varistors by post-annealing," *J. Mater. Res.*, vol. 13, no. 06, pp. 1560–1567, Jan. 2011.

[6] S. J. So and C. B. Park, "Analysis of the degradation characteristics using EPMA and the ambient sintering process in semiconducting ZnO ceramic varistors," *Journal-Korean Phys. Soc.*, vol. 38, no. 4, pp. 416–419, 2001.

[7] M. Takada, Y. Sato, and S. Yoshikado, "Effect of heat treatment on tolerance characteristic for electrical degradation of ZnO varistors with added Sb_2O_3," *Electr. Eng. Japan*, vol. 179, no. 2, pp. 1–10, 2012.

[8] Y. Akiyama, M. Takada, A. Fukumori, Y. Sato, and S. Yoshikado, "Effect of ZrO_2 Addition on Tolerance Characteristics of the Electrical Degradation of ZnO Varistors," *IEE J Trans. Fundam. Mater.*, vol. 129, pp. 320–326, 2009.

[9] T. K. Gupta and W. G. Carlson, "A Grain-Boundary Defect Model for Instability Stability Of A Zno Varistor," *J. Mater. Sci.*, vol. 20, no. 10, pp. 3487–3500, 1985.

[10] M. Takada and S. Yoshikado, "Relation between grain boundary and electrical degradation of ZnO varistors," in *Key Engineering Materials*, 2006, vol. 320, pp. 117– 120.

[11] M. Science-Poland, "The effect of aluminum additive on the electrical properties of ZnO varistors," *Mater. Sci.*, vol. 27, no. 4, pp. 1208–1218, 2009.

[12] M. G. M. Sabri, B. Z. Azmi, Z. Rizwan, M. K. Halimah, M. Hashim, and M. H. M. Zaid, "Effect of temperature treatment on the optical characterization of ZnO-Bi_2O_3-TiO_2 varistor ceramics," *Int. J. Phys. Sci.*, vol. 6, no. 6, pp. 1388–1394, 2011.

[13] A. Badev, S. Marinel, R. Heuguet, E. Savary, and D. Agrawal, "Sintering behavior and non-linear properties of ZnO varistors processed in microwave electric and magnetic fields at 2.45GHz," *Acta Mater.*, vol. 61, no. 20, pp. 7849–7858, 2013.

[14] C.-W. Nahm, "Low-temperature sintering effect on varistor properties of ZnO–V_2O_5– MnO_2–Nb_2O_5–Bi_2O_3 ceramics," *Ceram. Int.*, vol. 39, no. 2, pp. 2117–2121, Mar. 2013.

[15] A. J. I. A. H. R. M. A. I. Khadim, "The Influence of Dy_2O_3 doping on the Electrical Properties of ZnO-Based Varistor," *J. Nat. Sci. Res.*, vol. 5, no. 6, pp. 2225–0921, 2015.

[16] H. Ik, O. Jin, and H. Kim, "Effect of Sb_2O_3 addition on the varistor characteristics of $ZnOBi_2O_3$ -ZrO_2 -M_{tr} O (M_{tr} = Mn, Co)," *J Electroceramics*, vol. 17, pp. 1083–1086, 2006.

[17] C. S. Chen, "Effect of the dopant valence state of Mn-ions on the microstructures and nonlinear properties of microwave sintered ZnO-V_2O_5 varistors," *J. Mater. Sci.*, vol. 38, no. 5, pp. 1033–1038, 2003.

[18] A. H. Khafagy, S. M. El-rabaie, M. T. Dawoud, and M. T. Attia, "Microhardness, microstructure and electrical properties of ZVM ceramics," *J. Adv. Ceram.*, vol. 3, no. 4, pp. 287–296, 2014.

[19] R. Guo, L. Fang, H. Zhou, X. Chen, D. Chu, B. Chan, and Y. Qin, "SbVO4 doped ZnO– V_2O_5-based varistor ceramics: microstructure, electrical properties, and conductive mechanism," *J. Mater. Sci. Mater. Electron.*, vol. 24, no. 8, pp. 2721–2726, 2013.

[20] F. Jiang, Z. Peng, Y. Zang, and X. Fu, "Progress on rare-earth-doped ZnO-based varistor materials," *J. Adv. Ceram.*, vol. 2, no. 3, pp. 201–212, 2013.

[21] K. Eda, "Zinc oxide varistors," *IEEE Electr. Insul. Mag.*, vol. 5, no. 6, pp. 28–30, 32, 1989.

[22] H. H. Hng and K. M. Knowles, "Characterisation of $Zn_3(VO_4)_2$ Phases in V_2O_5 -doped ZnO Varistors," vol. 19, pp. 721–726, 1999.

[23] C.-W. Nahm, J.-A. Park, B.-C. Shin, and I.-S. Kim, "Electrical properties and DC-Ceram. Int. 30, 1009 (2004)," *Ceram. Int.*, vol. 30, no. 6, pp. 1009–1016, Jan. 2004.

[24] J. Ott, A. Lorenz, M. Harrer, E. A. Preissner, C. Hesse, A. Feltz, A. H. Whitehead, and M. Schreiber, "The influence of Bi_2O_3 and Sb_2O_3 on the electrical properties of ZnO-based varistors," *J. electroceramics*, vol. 6, no. 2, pp. 135–146, 2001.

[25] C.-W. Nahm, "Major effect on electrical properties and aging behavior of ZnO–Pr6O11based varistor ceramics with small In_2O_3 doping changes," *J. Mater. Sci. Mater. Electron.*, vol. 23, no. 9, pp. 1715–1721, 2012.

[26] M. Wang, Q. Tang, and C. Yao, "Electrical properties and AC degradation characteristics of low voltage ZnO varistors doped with Nd 2 O 3," *Ceram. Int.*, vol. 36, no. 3, pp. 1095– 1099, 2010.

[27] C.-W. Nahm, "Microstructure, electrical properties, and aging behavior of ZnO–Pr6O11–CoO–Cr_2O_3–Y_2O_3–Er_2O_3 varistor ceramics," *Ceram. Int.*, vol. 37, no. 8, pp. 3049–3054, 2011.

[28] M. Wang, C. Yao, and N. Zhang, "Degradation characteristics of low-voltage ZnO varistor manufactured by chemical coprecipitation processing," *J. Mater. Process. Technol.*, vol. 202, no. 1–3, pp. 406–411, Jun. 2008.

[29] K. Eda, A. Iga, and M. Matsuoka, "Degradation mechanism of non-Ohmic zinc oxide ceramics," *J. Appl. Phys.*, vol. 51, no. 5, p. 2678, 1980.

[30] Y.-M. Chiang, "Compositional changes adjacent to grain boundaries during electrical degradation of a ZnO varistor," *J. Appl. Phys.*, vol. 53, no. 3, p. 1765, 1982.

[31] N. R. D'Amico, G. Cantele, and D. Ninno, "First-principles calculations of clean and defected ZnO surfaces," *J. Phys. Chem. C*, vol. 116, no. 40, pp. 21391–21400, 2012.

[32] G. W. Tomlins, J. L. Routbort, and T. O. Mason, "Zinc self-diffusion, electrical properties, and defect structure of undoped, single crystal zinc oxide," *J. Appl. Phys.*, vol. 87, no. 1, p. 117, 2000